

High-Power High-Isolation RF-MEMS Switches with Enhanced Hot-switching Reliability Using A Shunt Protection Technique

Yuhao Liu, Yusha Bey, and Xiaoguang Liu, *Member, IEEE*

Abstract—This paper presents a shunt protection technique to improve the hot-switching reliability of metal-contact radio-frequency micro-electromechanical (RF-MEMS) switches. The proposed technique places shunt protection contacts in front of the main contact of an RF-MEMS metal contact switch to block RF signal while the main contact is switching on or off. The shunt protection contact creates a local cold-switching condition for the main contact to increase the lifetime of the switch under hot-switching condition. The shunt protection technique can also increase the overall isolation of the switch. To demonstrate the technique, RF-MEMS switches with and without shunt protection were fabricated using all metal process. Compared with unprotected switch, the protected switch has longer lifetime under hot-switching condition. The protected switch has >100 million cycles and up to 500 million cycles lifetime under 1-W hot-switching condition, measured in open-air lab environment. Besides, the isolation of the shunt-protected switch is 70 dB at 1.0 GHz and 36 dB at 40 GHz, and insertion loss is 0.30 dB at 1.0 GHz and 0.43 dB at 40 GHz.

Index Terms—RF MEMS, MEMS switch, RF micro-electromechanical systems, MEMS reliability, hot-switching

I. INTRODUCTION

METAL-CONTACT radio-frequency microelectromechanical switches exhibit superior RF performance in terms of bandwidth, linearity, insertion loss, power consumption, and isolation [1]–[5]. Metal-contact RF-MEMS switches have been demonstrated by several research groups [6]–[12] and are also actively being commercialized by several companies. Despite the promising RF performances, conventional designs of metal-contact RF-MEMS switches often suffer from reliability issues, leading to a limited lifetime and uncertain mean-time-to-failure [13]–[20]. Among all the reliability issues, hot-switching damage is one of the limiting factors [21]–[28]. The hot-switching condition refers to when the switch turns on and off without turning off the RF signal. Compared to cold-switching, hot-switching incurs additional damages to the switch contacts. The main damage mechanisms include (a) field evaporation at small separations between contacts; (b) field emission at small separations which leads to heating from electron bombardment, followed by either melting or evaporation of contact material; (c) electromigration; (d) formation

of plasma comprising metal ions, followed by ions attracted toward the cathode [21]. These additional damages are caused by a local potential difference between the top contact dimple and bottom electrode during hot-switching.

In our previous work [29], we have proposed and experimentally validated a series protection technique to improve the hot-switching reliability by connecting the input port and output port with a secondary protective contact to lower the voltage potential difference before the main contact turns on and off. However, since the protection contact and the main contact are in parallel, the total off-state capacitance increases, leading to a decrease in the off-state isolation.

To remedy this shortcoming, we propose a shunt protection scheme in which the protection contacts are placed in shunt between the signal and the ground. This technique drastically improves the OFF-state isolation without significant reduction in the effectiveness of the protection. We present a detailed analysis to compare the performance between the series and shunt protection schemes. As a demonstration vehicle, we present a shunt-protected RF-MEMS switch design that achieves comparable hot-switching lifetime but significantly better off-state isolation when compared with a series-protected switch. In Section II the analysis and design of the switches are presented, and in Section III the experimental verification of the proposed structure is reported and discussed.

II. ANALYSIS AND DESIGN

A. Device Operation Concept

Fig. 1 and Fig. 2 show the working principle of the shunt protection technique, and comparing it with our previously reported series protection technique. The proposed switch in this paper goes through three states to transit from the initial state to on state. Fig. 2(a) shows the initial state of the switch when both the shunt protection contact and main contact are open. By closing the shunt protection contact, the device enters the high-isolation state shown in Fig. 2(b). In this state, the switch remains off. Because the incoming RF power is shunted to ground by the protection contact, the off-state isolation significantly improves. The shunt contact lowers the RF voltage swing on the main contact, therefore protecting it from hot-switching damage.

In the next step, the device enters the transition state by closing the main contact (Fig. 2(c)). Both the shunt protection contact and main contact are closed in this state. The shunt switch then opens, and the device enters the on state

Y. Liu and X. Liu are with the Department of Electrical and Computer Engineering, University of California at Davis, Davis, CA 95616 USA (e-mail: yuhliu@ucdavis.edu; lxgliu@ucdavis.edu).

Y. Bey is with the Center for Nano-MicroManufacturing, University of California at Davis, Davis, CA 95616 USA (e-mail: jasmall@ucdavis.edu).

Manuscript received November 06, 2016; revised January 22, 2017. This work was in part funded by Grant #1444086 of the Enhanced Access to Radio Spectrum (EARS) Program of the National Science Foundation.

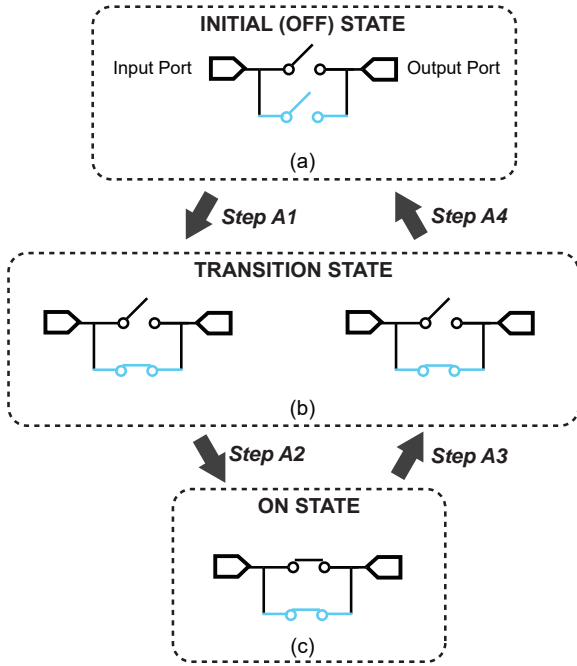


Fig. 1. Concepts of (a)-(c) Series-protection scheme [29].

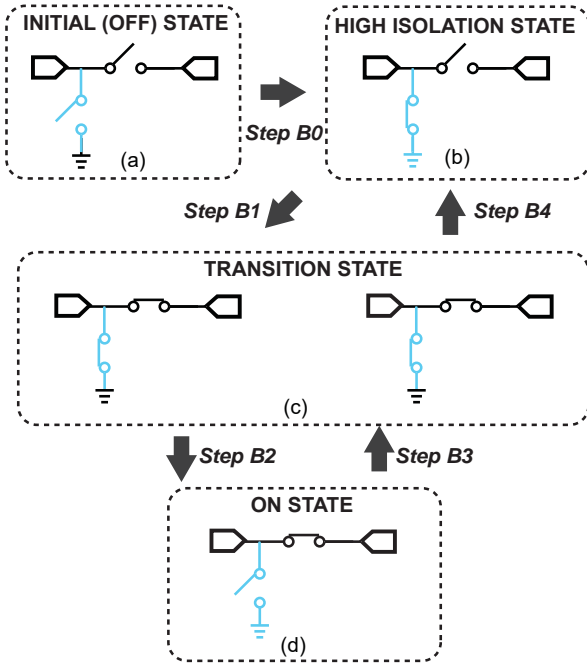


Fig. 2. Concepts of (a)-(d) The proposed shunt-protection scheme for hot-switching life-time enhancement.

(Fig. 2(d)). To switch from the on state to the high-isolation state, the process is reversed, and the main contact remains protected.

The effectiveness of the proposed protection scheme stems from the low electric field on the main contact as a result of the short circuit created by the shunt contact. Although the shunt contact will experience hot-switching damage, it can be

designed specifically to withstand such damage. For example, the shunt contact may be made from refractory metals that exhibit much higher hardness and therefore better immunity to hot-switching damage. Alternatively, the shunt contact may also be realized as with a solid-state switch using a high-voltage process for even better life-time enhancement.

Compared to the series protection scheme (Fig. 1(a)-(c)), the shunt-protection scheme offers improved isolation without significantly affecting the protection effectiveness. The following sections analyze in detail about the RF and lifetime performances of the proposed shunt protection scheme.

B. Comparison Between Shunt Protected Switch and Unprotected Switch (From off to on/ on to off)

The shunt protection contact can significantly lower the electric field intensity on the main contact during hot-switching. Fig. 3 shows the equivalent circuit model of an unprotected switch and a switch with shunt protection, when the main contacts transit from open to close (or from close to open) Fig. 2 (Step B1, B4). R_p models the contact resistance of the shunt protection contact. The main contact on the unprotected switch and the protected switch can be modeled as a variable parallel plate capacitor C_m with a varying gap d between the top and bottom electrode. The protection contact of the shunt-protected switch can also be modeled as variable parallel plate capacitor C_p

$$\begin{aligned} C_m &= \epsilon \frac{A_m}{d}, \\ C_p &= \epsilon \frac{A_p}{d}, \end{aligned} \quad (1)$$

where ϵ is the permittivity of the air, A_m and A_p are the overlap between top and bottom electrode, and d is the gap between the top electrode and the bottom electrode. The series inductance and parasitic capacitance are omitted for simplicity. The dimple area is much smaller than the overlap, so the dimple is also omitted in the total capacitance calculation of the contact area. ANSYS Maxwell simulation was carried out to find the limitation of the assumption, shown in Fig. 4. The capacitance of the parallel plates with contact dimple are higher than the simplified model, mainly because of the additional metal protrusion on the top plate. Without loss of generality, we use the parallel plate capacitance approximation for simplicity.

The S-parameters of the unprotected switch (Fig 3(a)) are [30]

$$S_{11} = \frac{1}{1 + 2j\omega Z_0 C_m}, \quad (2)$$

$$S_{12} = \frac{2j\omega Z_0 C_m}{1 + 2j\omega Z_0 C_m}, \quad (3)$$

where ω is the angular frequency of the RF signal, and $Z_0 = 50 \Omega$ is the characteristic impedance of the transmission line.

The voltage (peak voltage) across the switch contacts with an input power of P coming into the switch is

$$V_{sw} = V_1^- + V_1^+ - V_2^- = (S_{11} + 1 - S_{12})V_1^+, \quad (4)$$

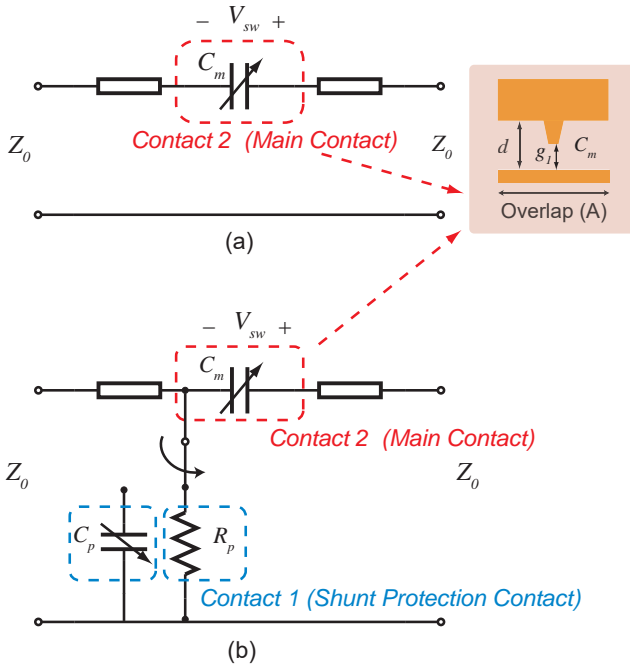


Fig. 3. Equivalent circuit of (a) Switch without protection at the moment of main contact hot-switching; (b) Switch with shunt protection at the moment of main contact hot-switching Fig. 2 (Step B1, B4).

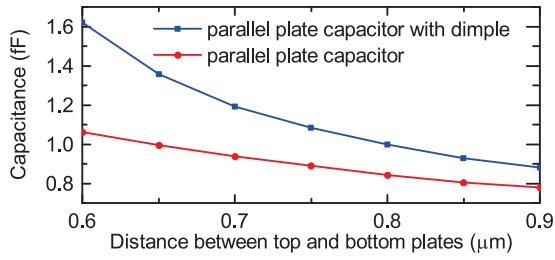


Fig. 4. ANSYSYS Maxwell simulation of capacitances of the parallel plates with contact dimple and the simplified parallel plates model under different gap distances.

where $V_1^+ = \sqrt{2PZ_0}$ is the amplitude of the incident wave (from the input port), V_1^- the amplitude of the reflected wave, V_2^- the amplitude of the transmitted wave, assuming that output port is matched.

The voltage $V_{sw,u}$ across the unprotected switch can then be calculated

$$V_{sw,u} = \sqrt{\frac{4}{4Z_0^2\omega^2C_v^2 + 1}} \cdot \sqrt{2PZ_0}. \quad (5)$$

In comparison, the S-parameters of the protected switch (Fig 3(b)) are

$$S_{11} = \frac{R_p - Z_0^2 j\omega C_m - Z_0}{2Z_0 R_p j\omega C_m + R_p + Z_0^2 j\omega C_m + Z_0}, \quad (6)$$

$$S_{12} = \frac{2Z_0 R_p j\omega C_m}{2Z_0 R_p j\omega C_m + R_p + Z_0^2 j\omega C_m + Z_0}, \quad (7)$$

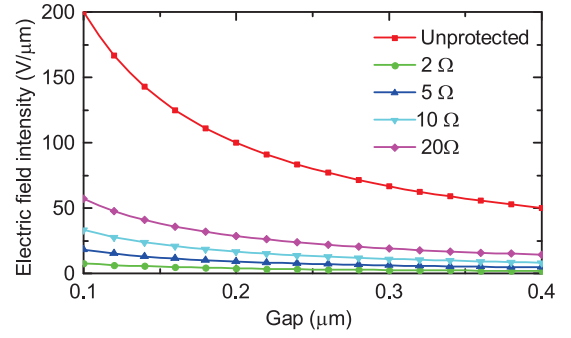


Fig. 5. Calculated electric field intensity of unprotected switch and switches with different shunt protection contact resistances.

The voltage across the main contact can be found using the same equation 4

$$V_{sw,m} = \sqrt{\frac{4}{(1 + \frac{Z_0}{R_p})^2 + (2Z_0 + \frac{Z_0^2}{R_p})^2 \omega^2 C_m^2}} \cdot \sqrt{2PZ_0}, \quad (8)$$

where R_p is the contact resistance of the shunt switch.

The electric field between the dimple area and the bottom electrode is

$$E_0 = \frac{V_{sw}}{g_1}, \quad (9)$$

where g_1 is the gap distance between the dimple area and the bottom electrode.

Fig. 5 shows a comparison of the maximum electric field intensity E_0 between the unprotected switch and shunt protected switch for several R_p values and gaps under 1 W power input. The calculation used device geometry parameters listed in Table I. Initial C_m was assumed to be 5 fF. The RF frequency used was 2.4 GHz. As the gap between the top contact dimple and the bottom contact electrode gets closer, the electric field intensity will increase for both switches. However, the electric field intensity of the main contact of the protected switch is significantly lower than that of the main contact of the unprotected switch.

The ratio (α) between the electric field intensity on the main contacts of the protected switch and the unprotected switch can be expressed as

$$\alpha = \frac{E_{maxsw,m}}{E_{maxsw,u}} = \sqrt{\frac{4Z_0^2\omega^2C_v^2 + 1}{(1 + \frac{Z_0}{R_p})^2 + (2Z_0 + \frac{Z_0^2}{R_p})^2 \omega^2 C_m^2}}. \quad (10)$$

Fig. 6 plots the ratio over different protection contact resistances. When the protection resistance is smaller than 20 Ω , the electric field intensity on the protected one is one third of that on the unprotected one. Thus, the main contact in the protected switch will have less damages caused by strong electric field during hot-switching. If the shunt protection resistance is smaller, more RF power will be reflected, making the electric field intensity on the main contact much smaller.

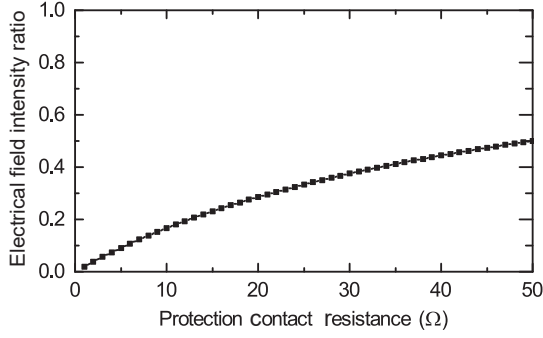


Fig. 6. Ratio between the electric field intensity on the main contacts of the protected switch and the unprotected switch.

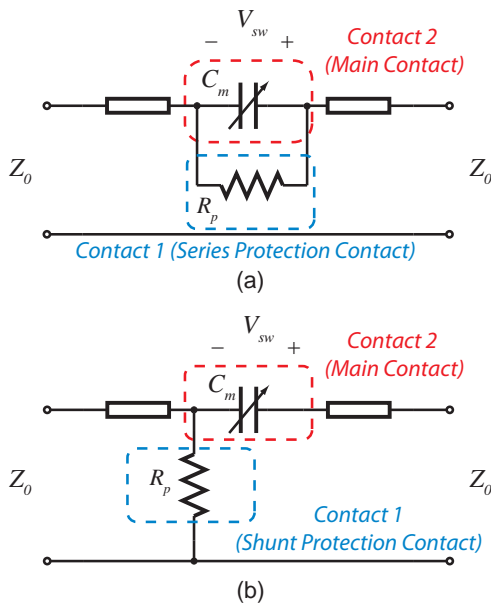


Fig. 7. Equivalent circuit of (a) switch with series protection at the moment of hot-switching Fig. 1 (Step A2, A3); (b) switch with shunt protection at the moment of hot-switching Fig. 2 (Step B1, B4).

C. Comparison Between Shunt-protected Switch and Series-protected Switch

Both the series protection [29] and shunt protection technique can provide hot-switching damage protection by lowering the electric field intensity on the main contact. Comparison between the two techniques will be discussed in this section.

Fig. 7 shows the circuit schematic of a series-protected switch and a shunt-protected switch at the moment when the main contact is closing (or opening), Fig. 1 (Step A2, A3) and Fig. 2 (Step B1, B4). The protection contacts of both switches are closed.

The voltages across the main contacts of both circuits in Fig 7(a) and (b) are

$$V_{sw,mseries} = \sqrt{\frac{8PZ_0}{(1 + \frac{2Z_0}{R_p})^2 + 4Z_0^2\omega^2C_m^2}}, \quad (11)$$

and

$$V_{sw,mshunt} = \sqrt{\frac{8PZ_0}{(1 + \frac{Z_0}{R_p})^2 + (2Z_0 + \frac{Z_0^2}{R_p})^2\omega^2C_m^2}}, \quad (12)$$

respectively.

Fig. 8 shows the comparison between the calculated electric field intensity of the main contacts of the series-protected and shunt-protected switches as the contact gap is closing (opening), for different protection contact resistances. The electric field intensity on the main contact of series-protected switch is approximately half of that on the shunt-protected switch. The initial C_m was assumed to be 5 fF. The RF frequency used was 2.4 GHz.

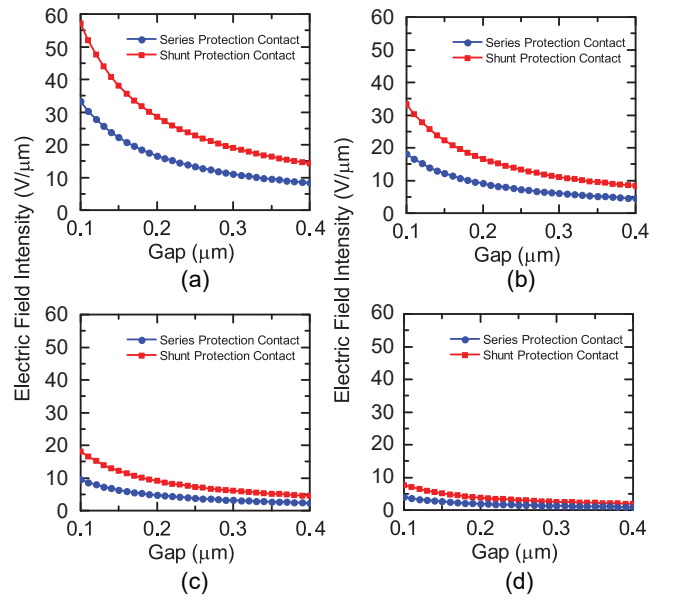


Fig. 8. Comparison between the calculated electric field intensity of the main contacts of the series-protected and shunt-protected switches when the protection contact resistances are (a) 20 Ω; (b) 10 Ω; (c) 5 Ω; (d) 2 Ω. The calculation assumes a center frequency of 2.4 GHz.

The electric field intensity on the protection contact when the protection contact is being closed (or open) can also significantly affect the overall lifetime of the switch, Fig. 1 (Step A1, A4) and Fig. 2 (Step B0). With directly exposed to higher electric field intensity, the protection contact could be worn out sooner. The contact resistance could increase faster over hot-switching cycles. High contact resistance of the protection contact will give less protection for the main contact, leading to a short overall lifetime of the switch. Fig. 9 shows the equivalent circuit of a series-protected switch and a shunt-protected switch before their protection contacts are closed.

For the series-protected switch in Fig. 9(a), the S-parameters are

$$S_{11} = \frac{1}{2Z_0j\omega(C_m + C_p) + 1}, \quad (13)$$

$$S_{12} = \frac{2Z_0j\omega(C_m + C_p)}{2Z_0j\omega(C_m + C_p) + 1}. \quad (14)$$

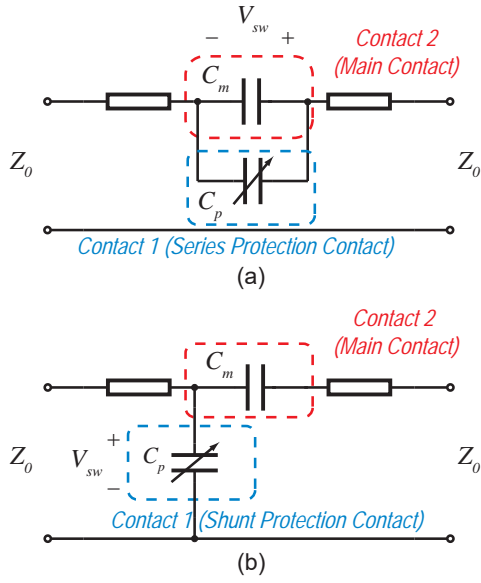


Fig. 9. Equivalent circuit of (a) Switch with series protection before the protection contact is closed (open) Fig. 1 (Step A1, A4); (b) Switch with shunt protection before the protection contact is closed (open) Fig. 2 (Step B0).

The voltage across the series protection contact is

$$V_{sw,series} = V_1^- + V_1^+ - V_2^- = (S_{11} + 1 - S_{12})V_1^+ \quad (15)$$

$$= \sqrt{\frac{4}{4Z_0^2\omega^2(C_p + C_m)^2 + 1}} \cdot \sqrt{2PZ_0}, \quad (16)$$

For the shunt-protected switch in Fig. 9(b), the S-parameters are

$$S_{11} = \frac{1 + \omega^2 C_m C_p Z_0^2 - Z_0 j \omega C_p}{2Z_0 j \omega C_m + 1 - Z_0^2 \omega^2 C_m C_p + Z_0 j \omega C_p}, \quad (17)$$

$$S_{12} = \frac{2Z_0 j \omega C_m}{2Z_0 j \omega C_m + 1 - Z_0^2 \omega^2 C_m C_p + Z_0 j \omega C_p}. \quad (18)$$

The voltage across the shunt protection contact is

$$V_{sw,pshunt} = V_1^- + V_1^+ = (S_{11} + 1)V_1^+ = \sqrt{2PZ_0} \cdot \frac{\sqrt{(2 + 4Z_0^2\omega^2 C_m^2)^2 + 4\omega^2 Z_0^2 (Z_0^2\omega^2 C_m^2 C_p + C_m + C_p)^2}}{(1 - Z_0^2\omega^2 C_m C_p)^2 + (2Z_0\omega C_m + Z_0\omega C_p)^2}. \quad (19)$$

The overlap between the top contact dimple and the bottom electrode is small. Thus, the capacitance is in the range of femto farad. If the device is operating in gigahertz range, it can be assumed that

$$Z_0\omega C_p \ll 1, \quad (20)$$

$$Z_0\omega C_m \ll 1, \quad (21)$$

$$Z_0\omega(C_p + C_m) \ll 1. \quad (22)$$

In this case, (16) and (19) can be simplified to

$$V_{sw,series} = V_{sw,pshunt} = 2\sqrt{2PZ_0}. \quad (23)$$

Essentially, the protection contacts on both series-protected and shunt-protected will have the same electric field intensity

damage during protection steps. The protection contacts on the series-protected switch will undergo this amount of high electric field intensity twice from off state to transition state and from transition state to off state Fig. 1 (Step A1, A4). The shunt protected contacts, however, can remain in close to leave the switch in high-isolation state (The switch does not necessarily go back to initial state.). Thus, the shunt-protected switch will only have one time switching from initial state to high-isolation state Fig. 2 (Step B0). The switching from initial state to high-isolation state can also happen in cold-switching condition to avoid any damage. However, the RF current will pass through shunt-protection contact at high-isolation state when the shunt-protection contact is prolongedly actuated, which makes the switch susceptible to adhesion problem at high-isolation state.

From transition state to on state (From on state to transition state) Fig. 2 (Step B2, B3), the protection contact will be open (close) and undergo addition hot-switching damage. Fig. 10 shows the equivalent circuit model of the shunt-protected switch when the protection contact is about to open (close), while the main contact is closed.

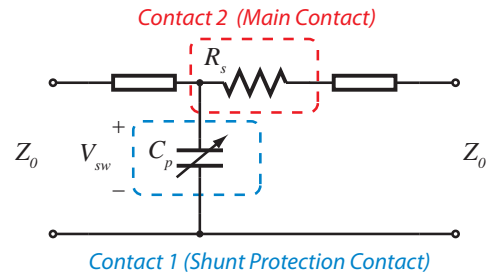


Fig. 10. Equivalent circuit model of the shunt-protected switch when the protection contact is about to open (close) while the main contact is closed Fig. 2 (Step B2, B3).

The S_{11} of the equivalent circuit is

$$S_{11} = \frac{R_s - Z_0 j \omega C_p - R_s Z_0 j \omega C_p}{2Z_0 + R_s + (Z_0^2 + Z_0 R_s) j \omega C_p}. \quad (24)$$

Then, the voltage across the shunt protection contact is

$$V_{sw,ushunt} = V_1^- + V_1^+ = (S_{11} + 1)V_1^+ = \sqrt{\frac{(2Z_0 + 2R_s)^2}{(2Z_0 + R_s)^2 + (Z_0^2 + Z_0 R_s)^2 \omega^2 C_p^2}} \cdot \sqrt{2PZ_0}. \quad (25)$$

Since $R_s \ll Z_0$ and $Z_0^2 \omega^2 C_p^2 \ll 1$, the equation can be simplified as

$$V_{sw,ushunt} = \sqrt{2PZ_0}. \quad (26)$$

Comparing (23) and (26), the electric field intensity during the hot-switching at Fig. 2 (Step B2) is half of the electric field intensity seen by the protection contact on series-protected switch during hot-switching. From on state back to transition state Fig. 2 (Step B3), the shunt protection contact will undergo the same hot-switching damage with the same electric field intensity. Overall, the electric field intensity during hot-switching on the protection contact of shunt-protected switch is half of the one on series-protected switch.

Fig. 11 plots the calculated S-parameter of a shunt-protected switch, a series-protected switch and an unprotected switch. The protection contact resistances is assumed to be $5\ \Omega$ for both shunt and series case in the calculation. $1\text{-}\Omega$ contact resistance is assumed for all main contacts. In the off state, it is assumed that the shunt protection contact is closed. In the on state, it is assumed that the series protection contact is closed. The calculation is based on simple estimation of equivalent circuit parameters from the switch design geometries listed in Table I. In particular, a simple parallel plate model is used to estimate the capacitance between the two electrodes. In practice, the actual capacitance would be larger due to parasitic capacitances. The parasitics would lead to a much higher calculated isolation. To simplified the analysis, the parasitic capacitances is neglected. All other parasitic capacitance and inductance are also ignored. From the calculation, it can be seen that in the off state the shunt-protected switch has better isolation, and the series-protected switch has worse isolation than the unprotected one because of the additional RF coupling of the capacitor formed in series protection contact. In the on state the shunt-protected switch has slightly higher insertion loss than the unprotected one since there is additional parasitic capacitance in shunt. The series-protected switch has better insertion because of the additional series protection contact.

In summary, the hot-switching electric field intensity on the main contact of shunt-protected switch is twice of that of the series-protected switch. The hot-switching electric field intensity on the protection contact of shunt-protected switch is half of that of the series-protected switch. Based on these two observations, we expect approximately similar lifetime enhancement from the series- and shunt-protection scheme, assuming that the lifetime of the contacts is directly related to electric field intensity. The advantage of the shunt-protected switch lies in its much better off-state isolation due to the series-shunt configuration.

D. Switch Design and EM Analysis

Fig. 12 and Table I show the design parameters of the switch. The device consists of three cantilever beams. The shunt protection switch beam length is slightly shorter than the main switch beam length to achieve faster switching speed. The main contact is made of gold to lower the contact resistance, and the shunt protection contact is made of refractory metal to withstand hot-switching damage. A compromise exists between the hardness of the contact and its contact resistance. In general, low-contact resistance materials, such as Au, Cu, and Ag, are all relatively soft and has a lower melting point than refractory metals. On the other hand, harder contact materials usually result in a higher contact resistance, leading to a degradation in the on-state insertion loss of the switch [17]. Mechanical stop dimple is designed to prevent the cantilever accidentally touching the biasing pad which can cause catastrophic failure of the switch. Dielectric film is not used within the biasing electrostatic field line to avoid any dielectric charging. An air bridge is formed to let the high-resistance biasing line pass through the ground plane.

The proposed switch design is simulated in ANSYS HFSS. Fig 13 shows the current distribution of the switch before and

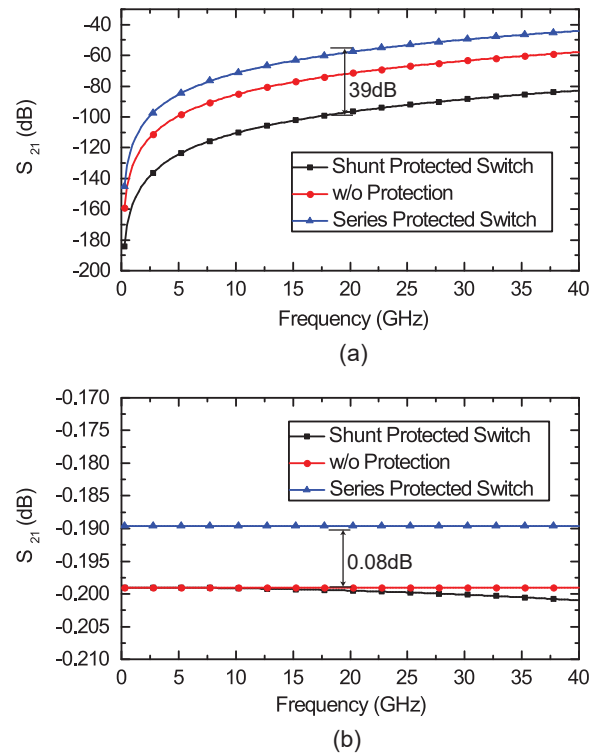


Fig. 11. Calculated S-parameter for (a) A shunt-protected switch, a series-protected switch and an unprotected switch at off-state; (b) A shunt-protected switch, a series-protected switch and an unprotected switch at on-state.

after the main switch is closed. The RF current is blocked by the shunt protection contact, and the main contact will meet less RF power and have less hot-switching damage. Fig. 14 shows the simulated S-parameters of the proposed design. According to the simulation results, the switch has better than 40 dB isolation in high-isolation state up to 40 GHz and better than 0.9 dB insertion loss in on state up to 40 GHz. The simulated S-parameter is very close to measurement results. The total area of the shunt-protected switch is larger than series-protected switch [29], but the overall size is still relatively small and approximately $400\ \mu\text{m} \times 300\ \mu\text{m}$. Signal integrity issues may not be a major factor for this design.

III. EXPERIMENTAL VALIDATION

A. Device Fabrication

The all-metal process [29] was used to fabricate the switch. The switches were fabricated on high-resistivity silicon wafer. The switch layer was isolated from silicon wafer by a $0.5\text{-}\mu\text{m}$ thermally grown oxide. 150-nm high-resistivity silicon chromium layer was patterned as DC biasing line. 150-nm gold layer was then deposited as low-resistance bottom contact. 50-nm platinum layer was deposited as protection bottom contact. The copper sacrificial layer was changed to chromium sacrificial layer. The chromium layer can withstand gold etchant in the following steps to ensure a cleaner process and higher fabrication yield. The use of the chromium layer also shrinks the total types of metal used in the all-metal process

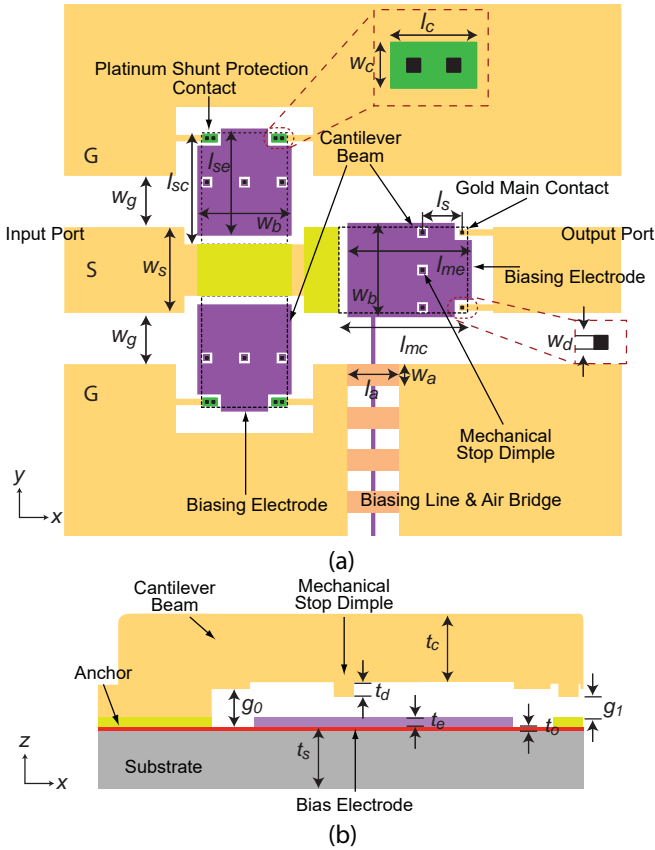


Fig. 12. (a) Top view of the shunt-protected switch; (b) Side view of the cantilever.

to four: gold, platinum, titanium and chromium. Gold beam structure and coplanar waveguide line were plated on the top of the sacrificial layers. The devices were released in chromium etchant and dried in critical point dryer. The fabricated devices are shown in Fig. 15. Both protected switch in Fig. 15(a) and unprotected switch in Fig. 15(b) are fabricated in parallel for comparison in tests later.

B. S-Parameters

The S-Parameters of the switch were measured by a Keysight 8722D network analyzer with Ground-Signal-Ground (GSG) microwave probes. The probes were calibrated to the reference line in Fig. 15(a) using Through-Reflection-Line (TRL) technique. The calibration kit was fabricated along side with the MEMS devices on the same wafer using the same process. The measured S-parameters, shown in Fig. 16, are close to the simulation results, and the switches were biased at 60 V. For the shunt-protected switch the isolation is 43.5 dB in the initial state, 72.3 dB in the high isolation state, and 25.8 dB in the transition state at 1.0 GHz. The isolation is 14.4 dB in the initial state, 36.0 dB in the high isolation state, and 22.1 dB in the transition state at 40 GHz. The isolation of the switch improves by 39.1 dB at 2.4 GHz. The insertion loss is 0.3 dB at 1 GHz and 0.48 dB at 40 GHz. For the unprotected switch, shown in Fig. 17, the isolation is 41.6 dB at 1 GHz and 14.1 dB at 40 GHz, and the insertion loss is 0.22 dB at 1 GHz

TABLE I
DESIGN PARAMETERS OF THE SWITCH

Geometry parameter	Symbol	Value (μm)
CPW line width	w_s	100
CPW line gap	w_g	60
Beam width	w_b	100
Dimple width	w_d	2.5
Electrode width	w_e	110
Shunt contact width	w_c	8.5
Air bridge width	w_a	25
Main switch beam length	l_{mc}	150
Shunt protection switch beam length	l_{sc}	130
Main switch electrode length	l_{me}	145
Shunt protection switch electrode length	l_{se}	125
Air bridge length	l_a	60
Stopper and main contact separation	l_s	45
Shunt contact width	l_c	16
Beam thickness	t_b	5
Dimple thickness	t_d	0.5
Biasing electrode thickness	t_e	0.15
Thermal oxide thickness	t_o	0.5
Substrate thickness	t_s	500
Cantilever to electrode gap	g_0	0.9
Dimple to contact gap	g_1	0.4
Electric parameter	Symbol	Initial Value (fF)
Main Contact parallel plate capacitor	C_m	5
Protection Contact parallel plate capacitor	C_p	5

and 0.25 dB at 40 GHz. The protected switch has significantly higher isolation (>30 dB) than the unprotected switch and similar insertion loss over 0–40 GHz range.

C. Linearity Test

The linearities of a protected switch and a through line were measured. Two-tone measurement setup is shown in Fig. 18(a). Two tones were offset by 25 MHz at center frequency of 2.4 GHz. The resolution bandwidth is 20 kHz. The input power is from 12 dBm to 16 dBm. The signal was attenuated by 20 dB before being sent into spectrum analyzer. The measured third order inter-modulation intercept point (IIP3) of the protected switch is 56.08 dBm, and that of the through line is 58.36 dBm.

D. Switching Time

Switching time is measured before lifetime measurement in order to determine the appropriate cycling frequencies. The switching time test, mechanical lifetime test and hot-switching lifetime test in later sections were all carried out in an open air, lab environment. The switching time measurement is carried out on a single cantilever switch without considering the sequential actuation of the protection and the main switches. Test setup is shown in Fig 19. A 2.4-GHz signal was sent from an RF signal generator to the device through a bias tee. The device was actuated by a square-wave biasing signal

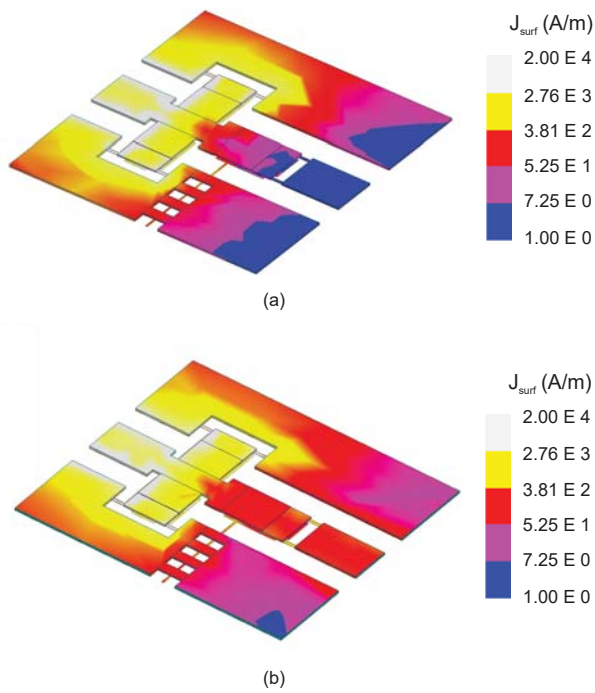


Fig. 13. (a) Current distribution of the switch after protection contact closed and before the main contact closed; (b) Current distribution of the switch after both contact closed.

that was generated by a function generator and amplified by a linear amplifier. Peak-to-peak voltage is 50 V and frequency is 100 Hz. The output RF signal from the MEMS switch was detected and converted to dc voltage by a zero-biased RF detector. The DC voltage and the biasing signal were sent to oscilloscope to determine the switching time. The switching-on time is 30.4 μs , and the switching-off time is 39.8 μs , as shown in Fig. 20. The shunt protection cantilever is slightly shorter than the main cantilever, so the switching time for the shunt protection cantilever should be shorter.

E. Mechanical Cycle Test

Mechanical lifetime test was carried out first before electrical lifetime test in order to verify the mechanical life time of the fabricated switches. Two switches were test without RF power passing through. The contact resistance was measured by 4-point resistance measurement setup during the switching cycles. The switches were biased using square wave with peak-to-peak voltage of 50 V and 50% duty cycle. The frequency was set to 1 kHz before 10,000 cycles and 5 kHz till the test stopped. The two switches were cycled up to 1.5 billion times before the test stopped. The resistance changes during the cycling test is shown in Fig. 21. The resistances of both switches gradually increase over time due to mechanical wear and damage, but are below 10 Ω after 1.5 billion cycles.

F. Hot-switching Lifetime Test

Hot-switching test setup is shown in Fig. 22. An amplified RF signal of 1 W at 2.4 GHz is sent to the device under test.

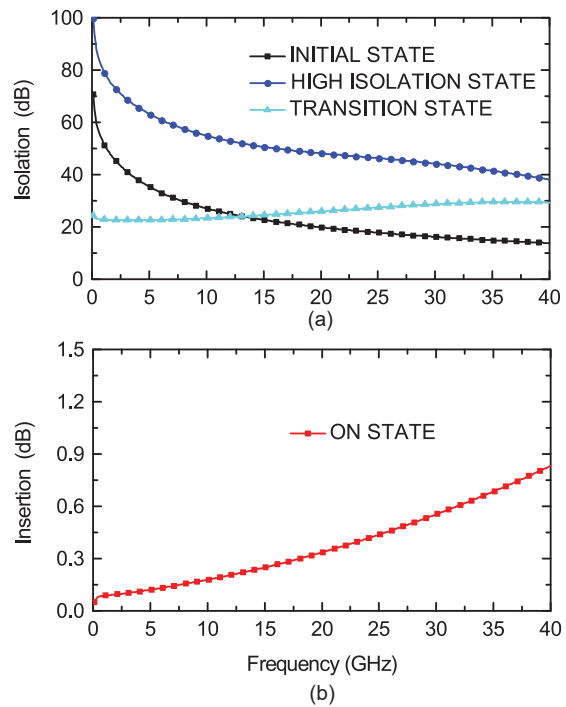


Fig. 14. Simulated (a) Isolation of the switch in initial state, high-isolation state, and transition state; (b) Insertion loss of the switch in the on state.

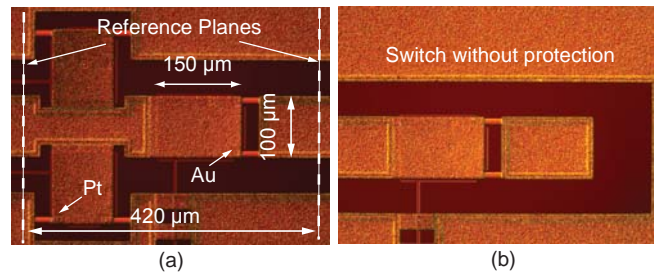


Fig. 15. Pictures of the (a) Protected switch and (b) Unprotected switch.

A power meter was connected through a 20-dB directional coupler to monitor the power level of the incoming RF signal. A 4-point resistance measurement setup is connected through bias tees to monitor the contact resistance changes over lifetime. The output RF signal is connected through a directional coupler to RF detector. The dc voltage is sent into an oscilloscope to monitor the switching behavior.

In the first case, an unprotected switch was tested. The amplified square wave with duty cycle of 50% and peak-to-peak voltage of 50 V. The frequency of the wave was set to 1 kHz before 10,000 cycles, and 5 kHz till the end of the test. Three unprotected devices were measured. Fig. 23 shows the resistance changes over the cycling period. The devices can be cycled up to 10 million cycles before failure. All switches failed as open circuit. The contact resistances became significantly large ($>200 \Omega$).

Next, the lifetime of the protected switches was measured under 1-W hot-switching condition. The shunt-protected switches are biased using the waveform (Fig. 24). The wave-

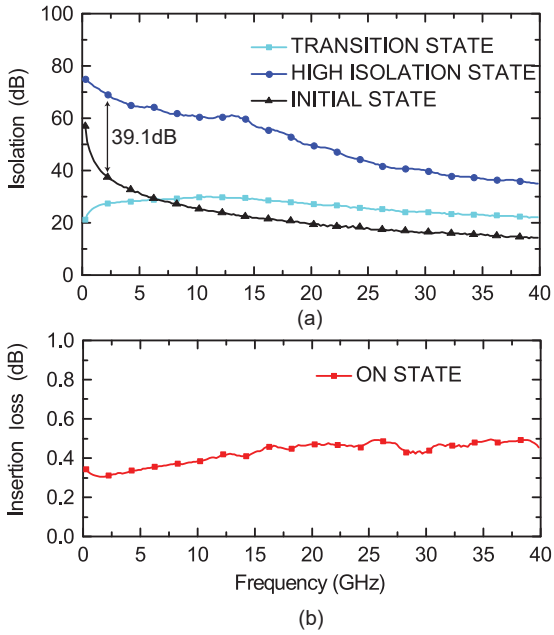


Fig. 16. Measured S-parameter of shunt-protected switch: (a) Isolation of initial state, high-isolation state, and transition state; (b) Insertion loss of on state.

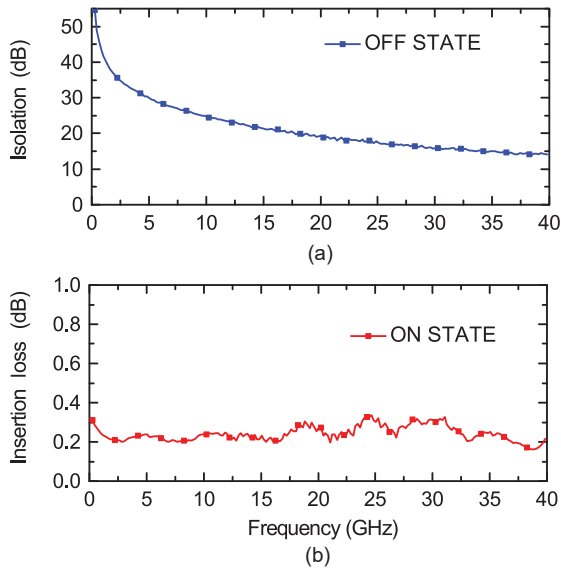


Fig. 17. Measured S-parameter of unprotected switch: (a) Isolation of off state; (b) Insertion loss of on state.

form consists of two identical sets of square waves which have a duty cycle of 66.7% and peak-to-peak voltage of 50 V. The phase of square wave that is used to bias the shunt protection contact has 180° lead on that used to bias the main contact to ensure that the shunt protect contact is closed when the main contact turns on and off, and that the shunt protect contact switches to open when the main contact is closed. The frequency of the biasing waveform was set to 333 Hz before 10,000 cycles, and 3,333 Hz till the end of the test.

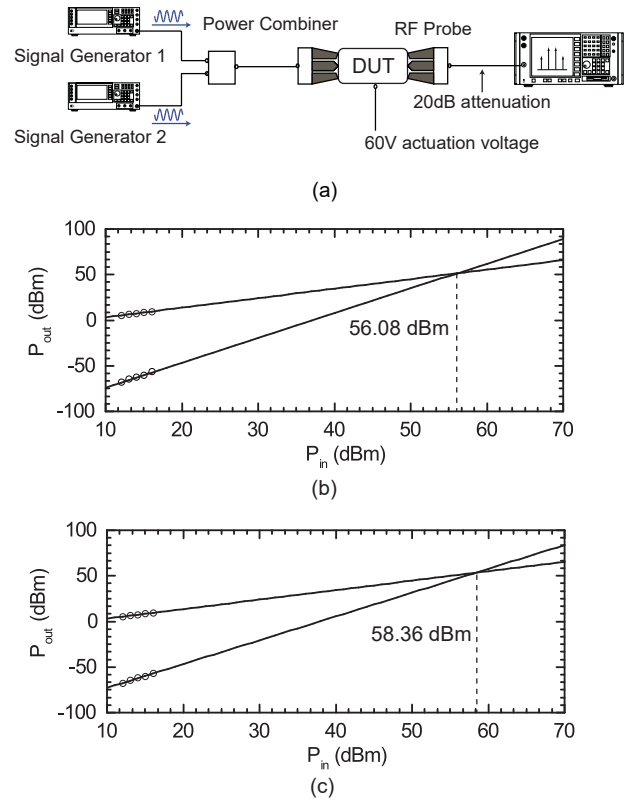


Fig. 18. (a) Linearity test setup; (b) IP3 of the shunt-protected MEMS switch; (c) IP3 of the through line.

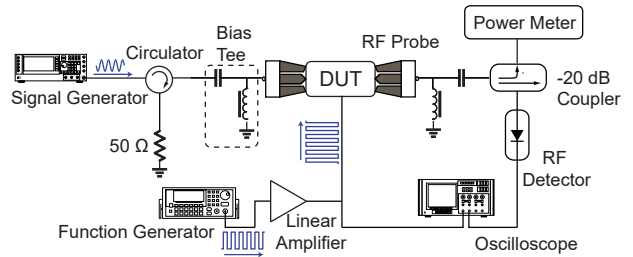


Fig. 19. Setup schematics for switching time measurement.

Three devices were tested, and the main contact resistance changes of the three measured devices are shown in Fig. 25. The lifetime of the switches increased to >100 million cycles. One of the switch lasted to 200 million cycles. The lifetime of the protected switch increases by at least 10 times than that of the unprotected switch. The changes of the protection contact resistance (R_p) were not measured. From the calculation in Section II (Fig 5), the electric field is at minimum when the R_p is the smallest because R_p effectively shorts the RF signal to ground. In this regard, the shunt protection contact is preferably made from low-resistance metals such as gold. However, in the proposed protection scheme, the main role of the shunt protection scheme is to withstand high RF voltage swing and a compromise must be made in the material choice.

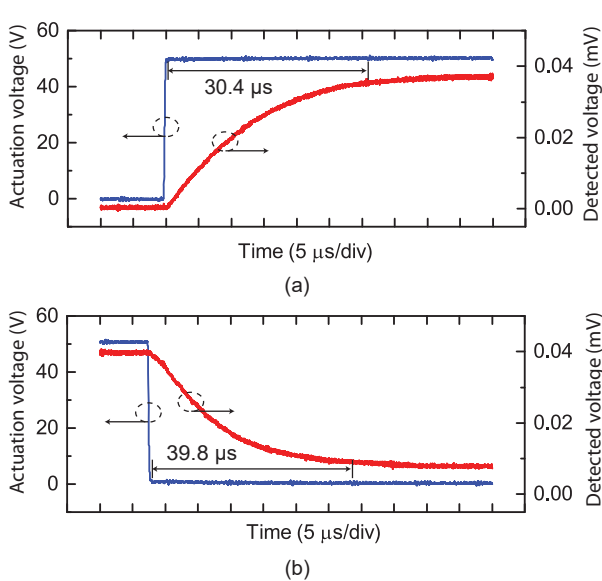


Fig. 20. (a) Switching-on time; (b) Switching-off time.

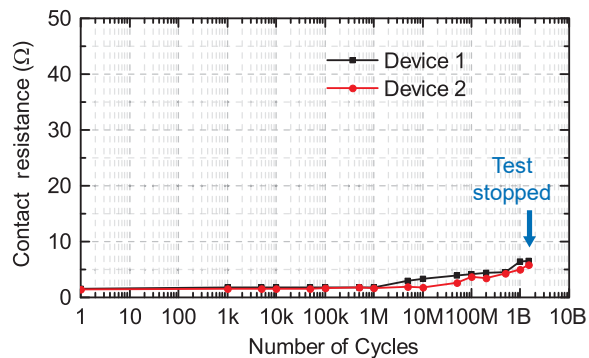


Fig. 21. Mechanical cycling test for two RF-MEMS switch devices (Test stopped after the last data points were collected).

Refractory metal is used in our work because it can provide better immunity to hot-switching damage due to their higher hardness, although at the penalty of higher contact resistance. In effect, a compromise must be made between the life-time of the main contact and the protection contact. The exact optimal point in terms of material choice and switch design will need further investigation. To lower the contact resistance of refractory metal contact, high contact force actuator can be used [25]. Another way to lower the contact resistance is to put several shunt-protection contacts in parallel. This will also lower the overall contact resistance, but insertion loss will also increase due to more on-state parasitics capacitance.

The lifetime of the protected switches under 1-W hot-switching condition was also measured when the shunt protection contact was always closed. This test is done to understand the lifetime of the main contact excluding the impact from the protection contact. In the test the shunt protection contact was continuously biased at 60 V, and the square wave has a peak-to-peak voltage of 50 V and duty cycle of 50 %. The frequency was set to 1 kHz before 10,000 cycles, and 5 kHz till the end

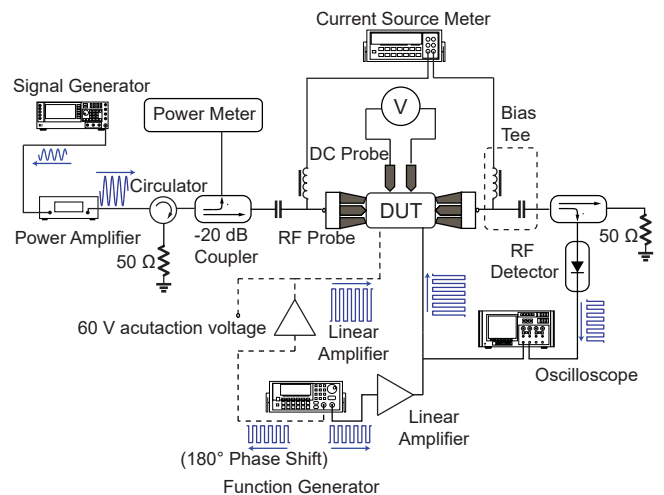


Fig. 22. Test setup for hot-switching reliability characterization.

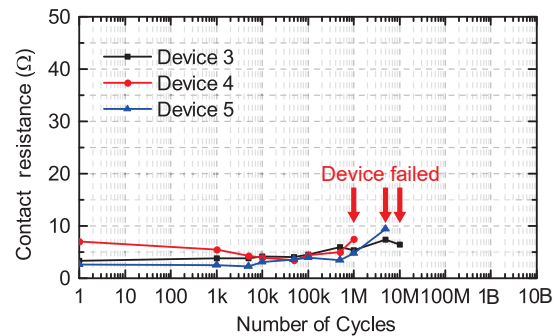


Fig. 23. Contact resistances changes over cycling period of three unprotected switches under 1-W hot-switching condition (All devices failed as open circuit at the next data points collection).

of the test. Fig. 26 shows the lifetime characterization of the device when the shunt protection contact is continuously held down. The lifetime can achieve >100 million cycles for all the three devices tested. Two of them reached >500 million cycles.

IV. CONCLUSION

A shunt protection technique to improve hot-switching reliability and isolation of RF-MEMS metal contact switch is presented in this paper. The comparisons between unprotected switch, shunt-protected switch and series-protected switch are theoretically analyzed. The experimental measurement shows both hot-switching reliability and isolation improvement by utilizing shunt protection technique, making the technique a robust method to improve RF-MEMS metal contact switch performance.

ACKNOWLEDGMENT

The authors would like to thank staff members in Center for Nano-Micro Manufacturing (CNM2) at the University of California, Davis, for help on device fabrication.

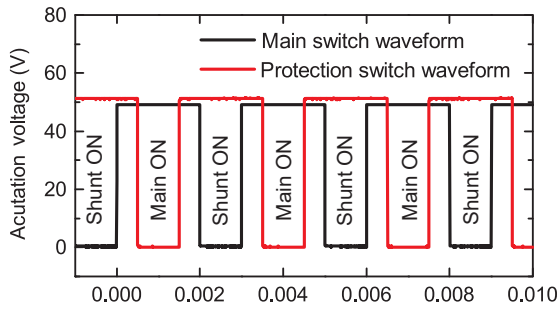


Fig. 24. Actuation waveform for the shunt protected switches.

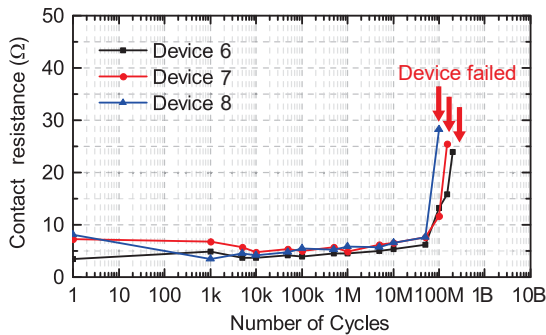


Fig. 25. Contact resistances changes over cycling period of three switches with shunt-protection using the actuation wave form shown in Fig. 24 under 1-W hot-switching condition (All devices failed as open circuit at the next data points collection).

REFERENCES

[1] E. R. Brown, "Rf-mems switches for reconfigurable integrated circuits," *IEEE Transactions on Microwave Theory and Techniques*, vol. 46, no. 11, pp. 1868–1880, Nov. 1998.

[2] J. Yao, "Rf mems from a device perspective," *Journal of Micromechanics and Microengineering*, vol. 10, no. 4, p. R9, 2000.

[3] G. R. et al, "Tuning in to rf mems," *IEEE Microwave Magazine*, vol. 10, no. 6, pp. 55–72, Oct. 2009.

[4] G. M. Rebeiz, C. D. Patel, S. K. Han, K. Chih-Hsiang, and K. M. J. Ho, "The Search for a Reliable MEMS Switch," *IEEE Microwave Magazine*, vol. 14, no. 1, pp. 57–67, Jan. 2013.

[5] P. Blondy and D. Peroulis, "Handling rf power: The latest advances in rf-mems tunable filters," *IEEE Microwave Magazine*, vol. 14, no. 1, pp. 24–38, Jan. -Feb. 2013.

[6] D. Peroulis, S. Pacheco, and L. Katehi, "RF MEMS switches with enhanced power-handling capabilities," *IEEE Transactions on Microwave Theory and Techniques*, vol. 52, no. 1, pp. 59–68, Jan. 2004.

[7] S. Gong, H. Shen, and N. Barker, "Study of Broadband Cryogenic DC-Contact RF MEMS Switches," *IEEE Transactions on Microwave Theory and Techniques*, vol. 57, no. 12, pp. 3442–3449, Dec. 2009.

[8] R. Stefanini, M. Chatras, P. Blondy, and G. Rebeiz, "Miniature MEMS Switches for RF Applications," *Journal of Microelectromechanical Systems*, vol. 20, no. 6, pp. 1324–1335, Dec. 2011.

[9] H. Zareie and G. Rebeiz, "Compact High-Power SPST and SP4T RF MEMS Metal-Contact Switches," *IEEE Transactions on Microwave Theory and Techniques*, vol. 62, no. 2, pp. 297–305, Feb. 2014.

[10] H. H. Yang, A. Yahiaoui, H. Zareie, P. Blondy, and G. M. Rebeiz, "Symmetric and compact single-pole multiple-throw (sp7t, sp11t) rf mems switches," *Journal of Microelectromechanical Systems*, vol. 24, no. 3, pp. 685–695, Aug. 2015.

[11] D. A. Czaplewski, C. D. Nordquist, G. A. Patrizi, G. M. Kraus, and W. D. Cowan, "RF MEMS Switches With RuO₂/Au Contacts Cycled to

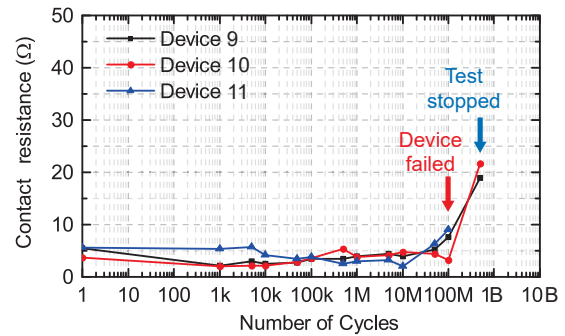


Fig. 26. Contact resistances changes over cycling period of three switches with shunt-protection contact continuously closed under 1-W hot-switching condition (One device failed as open circuit at the next data point collection, and for the other two devices test stopped after the last data points were collected).

10 Billion Cycles," *Journal of Microelectromechanical Systems*, vol. 22, no. 3, pp. 655–661, June 2013.

[12] Y. Liu, Y. Bey, and X. Liu, "Single-actuator shunt-series RF-MEMS switch," in *IEEE MTT-S International Microwave Symposium (IMS)*, 2014, pp. 1–4.

[13] D. Becher, R. Chan, M. Hattendorf, and M. Feng, "Reliability Study of Low-Voltage RF MEMS Switches," *GaAs MANTECH Conference*, pp. 54–57, 2002.

[14] P. Decuzzi, G. P. Demelio, G. Pascasio, and V. Zaza, "Bouncing dynamics of resistive microswitches with an adhesive tip," *Journal of Applied Physics*, vol. 100, no. 2, p. 024313, July 2006.

[15] M. Vincent, S. W. Rowe, C. Poulain, D. Mariolle, L. Chiesi, F. Houz, and J. Delamare, "Field emission and material transfer in microswitches electrical contacts," *Applied Physics Letters*, vol. 97, no. 26, 2010.

[16] H.-H. Hsu, M. Koslowski, and D. Peroulis, "An Experimental and Theoretical Investigation of Creep in Ultrafine Crystalline Nickel RF-MEMS Devices," *IEEE Transactions on Microwave Theory and Techniques*, vol. 59, no. 10, pp. 2655–2664, Oct. 2011.

[17] H. Kwon, D.-J. Choi, J.-H. Park, H.-C. Lee, Y.-H. Park, Y.-D. Kim, and H.-J. Nam, "Contact materials and reliability for high power rf-mems switches," *IEEE 20th International Conference on Micro Electro Mechanical Systems (MEMS)*, pp. 231–234, 2007.

[18] D. A. Czaplewski, C. D. Nordquist, C. W. Dyck, G. A. Patrizi, G. M. Kraus, and W. D. Cowan, "Lifetime limitations of ohmic, contacting RF MEMS switches with Au, Pt and Ir contact materials due to accumulation of friction polymer on the contacts," *Journal of Micromechanics and Microengineering*, vol. 22, no. 10, 2012.

[19] S. Patton and J. Zabinski, "Fundamental studies of Au contacts in MEMS RF switches," *Tribology Letters*, vol. 18, no. 2, pp. 215–230, 2005.

[20] A. Basu, G. G. Adams, and N. E. McGruer, "A review of micro-contact physics, materials, and failure mechanisms in direct-contact rf mems switches," *Journal of Micromechanics and Microengineering*, vol. 26, no. 10, p. 104004, 2016.

[21] R. P. Hennessy, A. Basu, G. G. Adams, and N. E. McGruer, "Hot-switched lifetime and damage characteristics of MEMS switch contacts," *Journal of Micromechanics and Microengineering*, vol. 23, no. 5, pp. 055 003–055 015, 2013.

[22] T. Ishida, K. Kakushima, and H. Fujita, "Degradation Mechanisms of Contact Point During Switching Operation of MEMS Switch," *Journal of Microelectromechanical Systems*, vol. 22, no. 4, pp. 828–834, 2013.

[23] A. Basu, R. Hennessy, G. Adams, and N. McGruer, "Reliability in Hot Switched Ruthenium on Ruthenium MEMS Contacts," in *IEEE 59th Holm Conference on Electrical Contacts (HOLM)*, 2013, pp. 1–8.

[24] Z. Yang, D. Lichtenwalner, A. Morris, J. Krim, and A. I. Kingon, "Contact degradation in hot/cold operation of direct contact micro-switches," *Journal of Micromechanics and Microengineering*, vol. 20, no. 10, p. 105028, Sep. 2010.

[25] C. D. Patel and G. M. Rebeiz, "A High-Reliability High-Linearity High-Power RF MEMS Metal-Contact Switch for DC to 40-GHz Applications," *IEEE Transactions on Microwave Theory and Techniques*, vol. 60, no. 10, pp. 3096–3112, Aug. 2012.

- [26] L. L. W. Chow, J. L. Volakis, K. Saitou, and K. Kurabayashi, "Lifetime Extension of RF MEMS Direct Contact Switches in Hot Switching Operations by Ball Grid Array Dimple Design," *IEEE Electron Device Letters*, vol. 28, no. 6, pp. 479–481, June 2007.
- [27] S. Yong-Ha, K. Min-Wu, L. Jeong Oen, K. Seung-Deok, and Y. Jun-Bo, "Complementary Dual-Contact Switch Using Soft and Hard Contact Materials for Achieving Low Contact Resistance and High Reliability Simultaneously," *Journal of Microelectromechanical Systems*, vol. 22, no. 4, pp. 846–854, April 2013.
- [28] S. Yong-Ha, K. Min-Wu, S. Min-Ho, and Y. Jun-Bo, "A complementary dual-contact mems switch using a zipping technique," *Journal of Microelectromechanical Systems*, vol. 23, no. 3, pp. 710–718, Sep. 2014.
- [29] Y. Liu, Y. Bey, and X. Liu, "Extension of the hot-switching reliability of rf-mems switches using a series contact protection technique," *IEEE Transactions on Microwave Theory and Techniques*, vol. 64, no. 10, pp. 3151 – 3162, Oct. 2016.
- [30] D. M. Pozar, *Microwave Engineering*, 4th ed. Wiley, New York, 2011.



Yuhao Liu received the B.Eng. degree in electrical engineering from McMaster University, Hamilton, ON, Canada, in 2011. He received his Ph.D. degree in electrical engineering at the University of California at Davis, Davis, CA, USA, in 2016. He is currently a senior electrical engineer in Skyworks Solutions.

His research interests include radio frequency micro-electromechanical (RF-MEMS) devices, THz interconnects, tunable filters, and active RF devices.



Yusha Bey received the Bachelor's degree in electrical engineering from Morgan State University, Baltimore, MD, USA, in 2005, and the Ph.D. degree from Purdue University, West Lafayette, IN, USA, in 2012.

He is currently the Lead Process Engineer for the Center for Nano-MicroManufacturing (CNM2) at University of California at Davis, Davis, CA, USA. His research interests include RF-MEMS for reconfigurable radio front ends.



Xiaoguang "Leo" Liu (S'07–M'10) received his B.S. degree from Zhejiang University, China in 2004 and his Ph.D. degree from Purdue University in 2010. He is currently an assistant professor in the Department of Electrical and Computer Engineering at the University of California at Davis.

His research interests include radio frequency micro-electromechanical (RF-MEMS) devices and other reconfigurable high frequency components, high frequency integrated circuits, and biomedical and industrial applications of high frequency communication and sensing systems.

communication and sensing systems.